




# Cancer-associated foam cells hamper protective T cell immunity and favor tumor progression in human colon carcinogenesis

Elena Daveri <sup>1</sup>, Barbara Vergani,<sup>2</sup> Luca Lalli,<sup>1</sup> Giulio Ferrero,<sup>3</sup> Elena Casiraghi <sup>4</sup>, Agata Cova,<sup>1</sup> Marta Zorza,<sup>1</sup> Veronica Huber <sup>1</sup>, Manuela Gariboldi,<sup>5</sup> Patrizia Pasanisi,<sup>6</sup> Simonetta Guarrera,<sup>7,8</sup> Daniele Morelli,<sup>9</sup> Flavio Arienti,<sup>10</sup> Marco Vitellaro,<sup>11</sup> Paola A Corsetto,<sup>12</sup> Angela M Rizzo,<sup>12</sup> Martina Stroschia,<sup>1</sup> Paola Frati,<sup>1</sup> Vincenzo Lagano,<sup>13</sup> Laura Cattaneo,<sup>13</sup> Giovanna Sabella,<sup>13</sup> Biagio E Leone,<sup>2</sup> Massimo Milione,<sup>13</sup> Luca Sorrentino,<sup>14</sup> Licia Rivoltini<sup>1</sup>

**To cite:** Daveri E, Vergani B, Lalli L, *et al.* Cancer-associated foam cells hamper protective T cell immunity and favor tumor progression in human colon carcinogenesis. *Journal for ImmunoTherapy of Cancer* 2024;**12**:e009720. doi:10.1136/jitc-2024-009720

► Additional supplemental material is published online only. To view, please visit the journal online (<https://doi.org/10.1136/jitc-2024-009720>).

LS and LR are joint senior authors.

Accepted 20 September 2024



© Author(s) (or their employer(s)) 2024. Re-use permitted under CC BY-NC. No commercial re-use. See rights and permissions. Published by BMJ.

For numbered affiliations see end of article.

## Correspondence to

Dr Elena Daveri;  
elena.daveri@istitutotumori.mi.it

Dr Licia Rivoltini;  
licia.rivoltini@istitutotumori.mi.it

## ABSTRACT

**Background** Colorectal cancer (CRC) remains a significant healthcare burden worldwide, characterized by a complex interplay between obesity and chronic inflammation. While the relationship between CRC, obesity and altered lipid metabolism is not fully understood, there are evidences suggesting a link between them. In this study, we hypothesized that dysregulated lipid metabolism contributes to local accumulation of foam cells (FC) in CRC, which in turn disrupts antitumor immunosurveillance.

**Methods** Tumor infiltrating FC and CD8<sup>+</sup> were quantified by digital pathology in patients affected by T2–T4 CRC with any N stage undergoing radical upfront surgery (n=65) and correlated with patients' clinical outcomes. Multiparametric high-resolution flow cytometry analysis and bulk RNAseq of CRC tissue were conducted to evaluate the phenotype and transcriptomic program of immune cell infiltrate in relation to FC accumulation. The immunosuppressive effects of FC and mechanistic studies on FC-associated transforming growth factor-beta (TGF-β) and anti-PD-L1 inhibition were explored using an in-vitro human model of lipid-engulfed macrophages.

**Results** FC (large CD68<sup>+</sup> Bodipy<sup>+</sup> macrophages) accumulated at the tumor margin in CRC samples. FC<sup>high</sup> tumors exhibited reduced CD8<sup>+</sup> T cells and increased regulatory T cells (Tregs). Functional transcriptional profiling depicted an immunosuppressed milieu characterized by reduced interferon gamma, memory CD8<sup>+</sup> T cells, and activated macrophages mirrored by increased T-cell exhaustion and Treg enrichment. Furthermore, FC<sup>high</sup> tumor phenotype was independent of standard clinical factors but correlated with high body mass index (BMI) and plasma saturated fatty acid levels. In CD8<sup>low</sup> tumors, the FC<sup>high</sup> phenotype was associated with a 3-year disease-free survival rate of 8.6% compared with 28.7% of FC<sup>low</sup> (p=0.001). In-vitro studies demonstrated that FC significantly impact on CD8 proliferation in TGF-β dependent manner, while inhibition of TGF-β FC-related factors restored antitumor immunity.

## WHAT IS ALREADY KNOWN ON THIS TOPIC

⇒ Dyslipidemia and obesity are major risk factors associated with colorectal cancer (CRC). Nonetheless, an insight of the immune-related mechanisms linking dysmetabolism and CRC progression is still warranted.

## WHAT THIS STUDY ADDS

⇒ In this study, we demonstrated that lipid-engulfed macrophages (foam cells (FC)) accumulate at primary lesion of patients with CRC in association with altered circulating plasma lipid profile and high body mass index (BMI), and restrain immunosurveillance by creating a T-cell hostile tumor milieu. FC quantification identifies a subset of patients with the highest risk of recurrence after surgery for stage I–III CRC.

## HOW THIS STUDY MIGHT AFFECT RESEARCH, PRACTICE OR POLICY

⇒ FC are a constant of chronic inflammation and cancer; however, their mechanisms in molding tumor immune microenvironment and blunting CD8<sup>+</sup> T cell-mediated cancer control is not well defined. Our findings provide deeper understanding of the mechanisms underlying the immune excluded phenotype in solid cancers and point to FC as a potential biomarker of aggressive disease, as well as a new target for therapy and prevention in patients with CRC.

**Conclusions** FC exert immunosuppressive activity through a TGF-β-related pathway, resulting in a CD8-excluded microenvironment and identifying immunosuppressed tumors with worse prognosis in patients with primary CRC. FC association with patient BMI and dyslipidemia might explain the link of CRC with obesity, and offers novel therapeutic and preventive perspectives in this specific clinical setting.

## INTRODUCTION

Despite significant advancements in the diagnosis and treatment of colorectal cancer (CRC), it remains the third leading cause of cancer-related death worldwide.<sup>1</sup> Emerging evidences suggest that dyslipidemia, increased body mass index (BMI), and obesity are major risk factors for CRC<sup>2</sup> indicating potential involvement of lipid-related disorders in gut carcinogenesis.<sup>3</sup> Conversely, the protective role of infiltrating CD8<sup>+</sup> T cells, assessed by their spatial distribution using the Immunoscore,<sup>4</sup> has been validated as a crucial feature in CRC, essential for adaptive antitumor immunity and for controlling tumor growth in immunogenic CRC.<sup>5</sup> Despite extensive research has explored the complex biological networks underlying human gut carcinogenesis,<sup>6</sup> the potential interplay between the tumor-favoring effects of dysregulated lipid metabolism, the protective T cell-mediated adaptive immunity, and their implications for CRC development remain poorly investigated.

Various immune cells located at the intestinal epithelium play pivotal roles in maintaining gut homeostasis.<sup>7</sup> In particular, colonic macrophages are increasingly acknowledged as key guardians, protecting the host from gastrointestinal pathogens while also promoting immune tolerance towards food and microbiota antigens.<sup>8,9</sup> The multifunctional properties of colonic macrophages, which are finely tuned both at local and systemic levels, are involved in the pathogenesis of numerous chronic gastrointestinal diseases, including inflammatory conditions and cancers.<sup>10,11</sup> Macrophages rely on lipid metabolism not only for cellular energy but also to adapt their phenotype and function.<sup>12</sup> By expressing scavenger receptors, these cells accumulate lipids in cytosolic droplets,<sup>13</sup> developing what is known as the “foam cells” (FC) morphology. While FC have been widely studied in the context of atherosclerosis<sup>14</sup> and tuberculosis,<sup>15</sup> they are increasingly recognized as a hallmark of chronic inflammation and is found in selected cancers, as well as in various metabolic, infectious, and autoimmune diseases.<sup>16</sup> Although the presence of FC in the bowel has been reported in specific pathological conditions, such as pediatric microscopic colitis,<sup>17</sup> and more recently, in scattered cases of CRC,<sup>18</sup> their immunological properties, particularly their impact on adaptive antitumor T cell immunity, remain largely unexplored. In non-cancerous pathological conditions, FC are known to exert immune-suppressive activity. This activity is associated with the induction of regulatory T cells (Tregs), a reduction in antigen-presenting capacity, and direct inhibition of CD8<sup>+</sup> T cell effectors through the release of transforming growth factor- $\beta$  (TGF- $\beta$ ) and other immunomodulating cytokines and chemokines.<sup>19,20</sup> Notably, many of these functional features are shared with tolerogenic colonic macrophages<sup>21</sup> and closely resemble the immunosuppressive activity observed in macrophages within the tumor microenvironment (TME).<sup>22</sup> This study aimed to investigate the role of FC and their altered lipid metabolism in impairing the protective effect of CD8 T cell immunity in

human CRC, exploring also their prognostic impact. The hypothesis driving this study is that colonic macrophages, engulfed by lipid excess, modulate T-cell infiltration to establish an immune-tolerant milieu that could facilitate cancer development and progression.

## METHODS

### Patients and sample collection

The study included prospective and retrospective cohorts of 65 patients (INT127/19 and INT149/19) with T2–T4, any N stage CRC treated with upfront surgery (online supplemental table S1). In-vitro mechanic studies were conducted using peripheral blood mononuclear cells (PBMCs) from healthy donors (HDs) (INT61/20).

### Immunohistochemistry and digital pathology assessment

Tumor specimens were assessed for the presence of CD68<sup>+</sup> and CD8<sup>+</sup> T lymphocytes, by immunohistochemistry. Formalin-fixed, paraffin-embedded (FFPE) tissue sections were evaluated using antigen retrieval, primary antibody incubation, and 3,3'-diaminobenzidine staining (EnVision FLEX System). High-resolution images were digitally scanned (Aperio Scanscope XT) and the whole tissues area was segmented using MiaQuant,<sup>23,24</sup> to quantify the cell marker-pixel densities in the tumor core (TC), adjacent mucosa (AM), invasive margin (IM) and distinct 400  $\mu\text{m}$ -thick region of interest, internal (intra) and peripheral (peri) from the IM. FC were identified as CD68<sup>+</sup> elements with an area greater than 100  $\mu\text{m}^2$ . Immunofluorescence (IF) staining was also used to detect CD68<sup>+</sup> Bodipy<sup>493/503+</sup> cells, CD8<sup>+</sup> T infiltrate, PD-1, Foxp3, TGF- $\beta$  and Ki67 markers. Images were captured by an Olympus BX63 microscope (online supplemental tables S2 and S3).

### Cell cultures

In vitro-derived FC were generated by culturing sorted CD14<sup>+</sup> cells from PBMCs of HDs and patients with CRC with macrophage colony-stimulating factor in absence or presence of oxLDL for 48 hours. T cell proliferation study was performed using CFSE staining prior TCR stimulation with anti-human CD3/CD28 mAb-conjugated beads and then cocultured at ratio 1:1 for 5 days with in vitro generated FC or monocyte-derived early macrophages as control, in presence or absence of anti-TGF- $\beta$ 1,2,3 and anti-PD-L1 mAbs (online supplemental table S3). Lymphocytes cultured alone were used as internal reference.

### Flow cytometry analyses

Flow cytometry assays were used to analyze single-cell suspensions derived from surgical specimens (n=21 CRC) and in vitro cell cultures. Surface antigens and intracellular lipid uptake were stained with fluorochrome-conjugated antibodies and reagents (online supplemental tables S3 and S4). Cytokine quantification was performed by Cytometric Bead Array. Samples were analyzed using

a CytoFLEX S flow cytometry (Beckman Coulter). Data analyses were conducted using the Kaluza Software (Beckman Coulter).

### Transcriptomic analyses

RNA was isolated from FFPE intestinal tissue sections of patients with CRC who underwent surgery and from cultured CD14<sup>+</sup> cells in the absence or presence of oxLDL for 48 hours. Library preparation was performed using Illumina Stranded Total RNA Prep according to the manufacturer's instructions. Sequencing and bioinformatics analyses (online supplemental table S5) were performed and annotated in the Gene Expression Omnibus (GEO) Super Series: GSE227206 and GSE273106.

### Lipidomic analyses

Total cholesterol, high-density lipoprotein (HDL), low-density lipoprotein (LDL), and triglycerides levels were analyzed using a Cobas Roche Automated Clinical Chemistry Analyzer (Roche Diagnostics), following standard clinical procedures. Plasma esterified fatty acids were analyzed as methyl esters. Quantification was performed using gas chromatograph equipped with a flame ionization detector, using the chromatographic peak area according to the internal standard method.

### Statistical analyses

Statistical analyses were performed using R software V.4.2.0 and GraphPad Prism (V.8.4.3), using either the Wilcoxon signed-rank test, two-tailed Mann Whitney U-test, two-way analysis of variance or Fisher's exact test. Correlation analyses were performed using Spearman's test. Statistical significance was set at  $p < 0.05$ . For survival analyses, Kaplan-Meier survival curves were generated, and a log-rank test was performed to assess statistical significance.

Detailed procedures are provided in online supplemental material section.

## RESULTS

### Baseline patients' characteristics

Mean age of patients with CRC ( $n=65$ ) was 69.1 ( $\pm 10.8$ ) years, 37 of which (56.9%) were male and 28 (43.1%) female. Mean BMI was 26.5 kg/m<sup>2</sup> (online supplemental table S1). Most patients had pT3 (70.8%), pN0 (55.4%), and G2 (75.4%) CRC. A right colectomy was performed in 18 cases (27.7%), a left colectomy in 20 (30.8%), and an anterior rectal resection in 27 patients (41.5%). None of them received neoadjuvant treatment. Adjuvant chemotherapy or chemo-radiotherapy was instead administered in 29 patients (44.6%) (online supplemental table S1).

### Macrophages accumulate lipid-droplets in primary CRC tissue

First, we investigated the presence of macrophages with lipid droplets in patients with stage I–III CRC. In tumor lesions, a subset of CD68<sup>+</sup> cells displayed a specific morphology of large polygonal cells with optically empty vacuoles-rich cytoplasm and centrally placed faint-colored

nuclei. The cytoplasmic vacuoles stained strongly positive for neutral lipids, and weakly positive for acidic mucins (figure 1A).

The accumulation of Bodipy<sup>+</sup> lipid droplets positively correlate with enhanced size of CD68<sup>+</sup> cells ( $p < 0.0001$ ), resembling macrophages turned into FC. Contrarily, CD68<sup>+</sup> macrophages displaying no lipid droplet content, which were reproducibly small in size, were defined as non-FC (figure 1B). Thus, a specific algorithm for digital pathology was developed to quantify FC and non-FC based on the morphology and size of CD68<sup>+</sup> elements, in the whole FFPE tissue section from the retrospective cohort, discriminating tumor core (TC), invasive margin (IM), and adjacent mucosa (AM) localization (figure 1C). Results from this analysis showed that FC accumulated at IM, displaying a “barrier-like” distribution. In contrast, non-FC were more ubiquitous, involving also intratumoral localizations and AM, and more homogeneously detected in the majority of patients (figure 1D(i)). Specifically, FC clustering was 54.2-fold higher at the IM than TC, while non-FC marker density showed an increase of 6.7-fold at the IM compared with TC ( $p < 0.0001$ ) (figure 1D(ii)).

Although clearly detectable along the tumor IM, the FC infiltrate was highly heterogenous among different patients (IQR: 0.006–0.035), allowing us to define a median cut-off value (0.02), and dichotomize the patients into the FC<sup>high</sup> (43%) versus FC<sup>low</sup> (57%) groups. While no association was observed between FC abundance and the main clinical and pathological variables, including CEA and CA19.9 levels, pT versus pN stages, and grading (online supplemental figure S1), a significant positive correlation was observed between FC accumulation in tissue and BMI (figure 1E). Conversely, BMI did not show any correlation with non-FC (online supplemental figure S1) and did not display a significant relationship with cancer-associated variables (online supplemental table S6). On this basis, we then investigated the association between FC infiltrate and plasma lipid profiles. FC<sup>high</sup> CRC exhibited a clustering with higher triglycerides and lower HDL in plasma compared with FC<sup>low</sup> CRC, while cholesterol and LDL did not show statistically significant differences between the two groups (online supplemental figure S2). Moreover, a thorough characterization of lipid species revealed elevated levels of saturated fatty acid, including palmitic acid (C16:0;  $p=0.04$ ) in FC<sup>high</sup> CRC. This group also displayed an enrichment of mono-unsaturated fatty acid ( $p < 0.0002$ ), specifically of oleic acid (C18:1;  $p < 0.0003$ ). In contrast, polyunsaturated fatty acids (PUFAs) were significantly lower in FC<sup>high</sup> tumors ( $p < 0.0076$ ), with no significant differences in omega-6 ( $n=6$ ) PUFA arachidonic acid (C20:4) while there a remarkable decrease of eicosapentaenoic acid (C20:5;  $p < 0.001$ ), docosapentaenoic acid (C22:5;  $p < 0.0006$ ), and docosahexaenoic acid (C22:6;  $p < 0.02$ ), both belonging to omega-3 ( $n=3$ ) PUFA, in FC<sup>high</sup> versus FC<sup>low</sup> CRC (figure 1F, online supplemental figure S2).



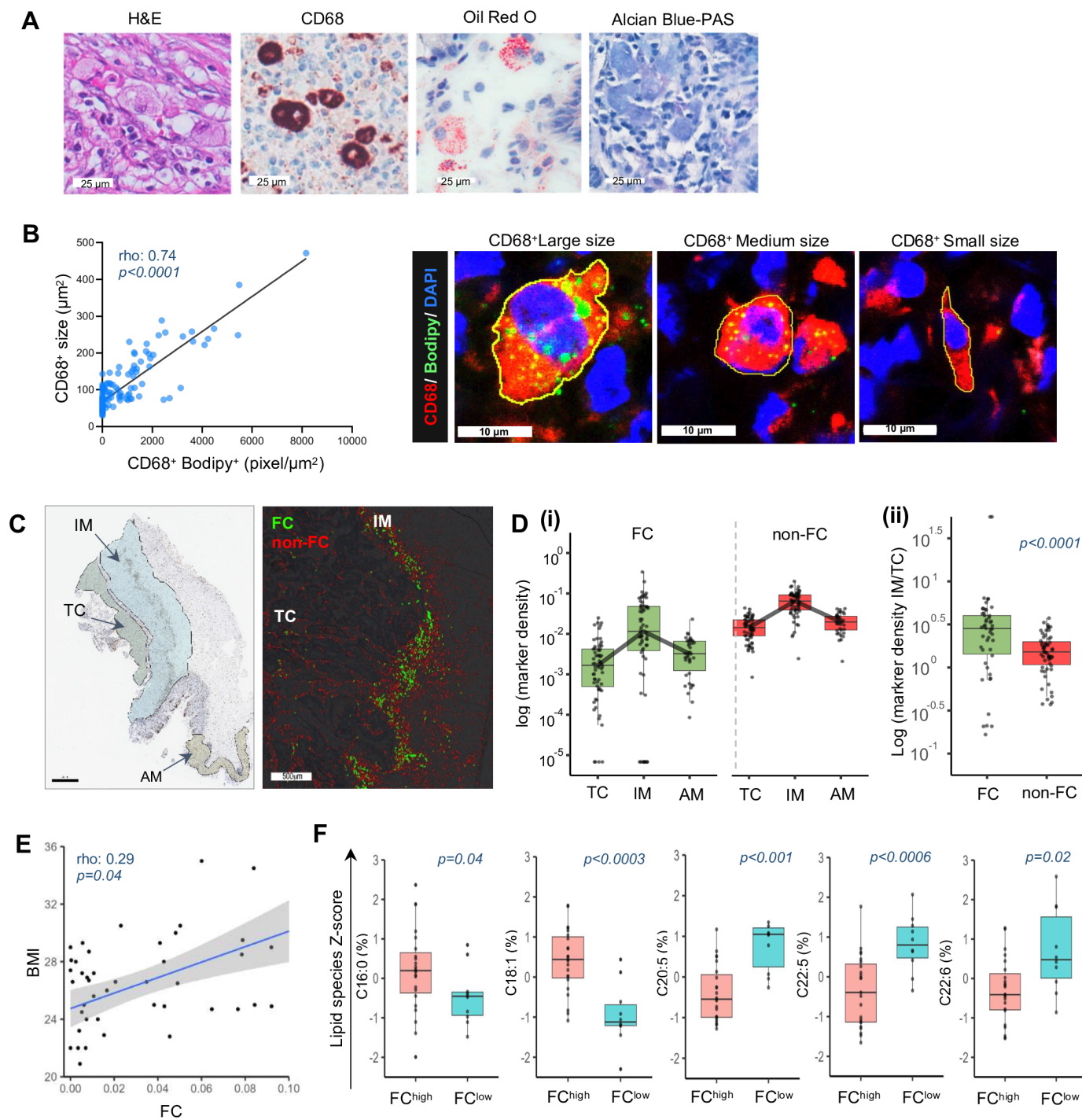


**Figure 1** Spatial distribution of cancer-associated foam cells (FC) in primary colorectal cancer (CRC). Representative images for H&E, CD68-, oil red O-, and Alcian blue PAS-stained sections in stage I-III CRC; (B) correlation plot of Bodipy<sup>493/503</sup> and cell size in tumor associated CD68<sup>+</sup> cells and relative confocal images (n=150 cells). (C) Representative images of FC and non-FC distribution across different tumor localization. Boxplots of (D(i)) FC (green) and non-FC (red) distribution across tumor core (TC), invasive margin (IM) and adjacent mucosa (AM), quantified by MiaQuant digital pathology, and (D(ii)) the IM/TC ratio of FC and non-FC. Values are expressed as logarithm of marker densities; (E) correlation between FC tissue accumulation and patient's body mass index (BMI); (F) boxplot of plasma lipid profile along FC<sup>high</sup> and FC<sup>low</sup> CRC obtained by K-means clustering methods. P values are determined by two-tailed Mann Whitney U-test.

### FC accumulation at the tumor edge prevents CD8<sup>+</sup> intratumoral infiltration

Next, CD8<sup>+</sup> T-cells were also quantified by digital pathology and tumors divided into CD8<sup>high</sup> (>0.025 median cut-off) and CD8<sup>low</sup> (<0.025) with respect to their

spatial distribution at IM. FC<sup>high</sup> CRC showed a significantly lower density of CD8<sup>+</sup> T cells, compared with FC<sup>low</sup> cases (p=0.04) (figure 2A(i)), and reciprocally, FC accumulation at IM was significantly higher in CD8<sup>low</sup> CRC (p=0.01) (figure 2A(ii)).

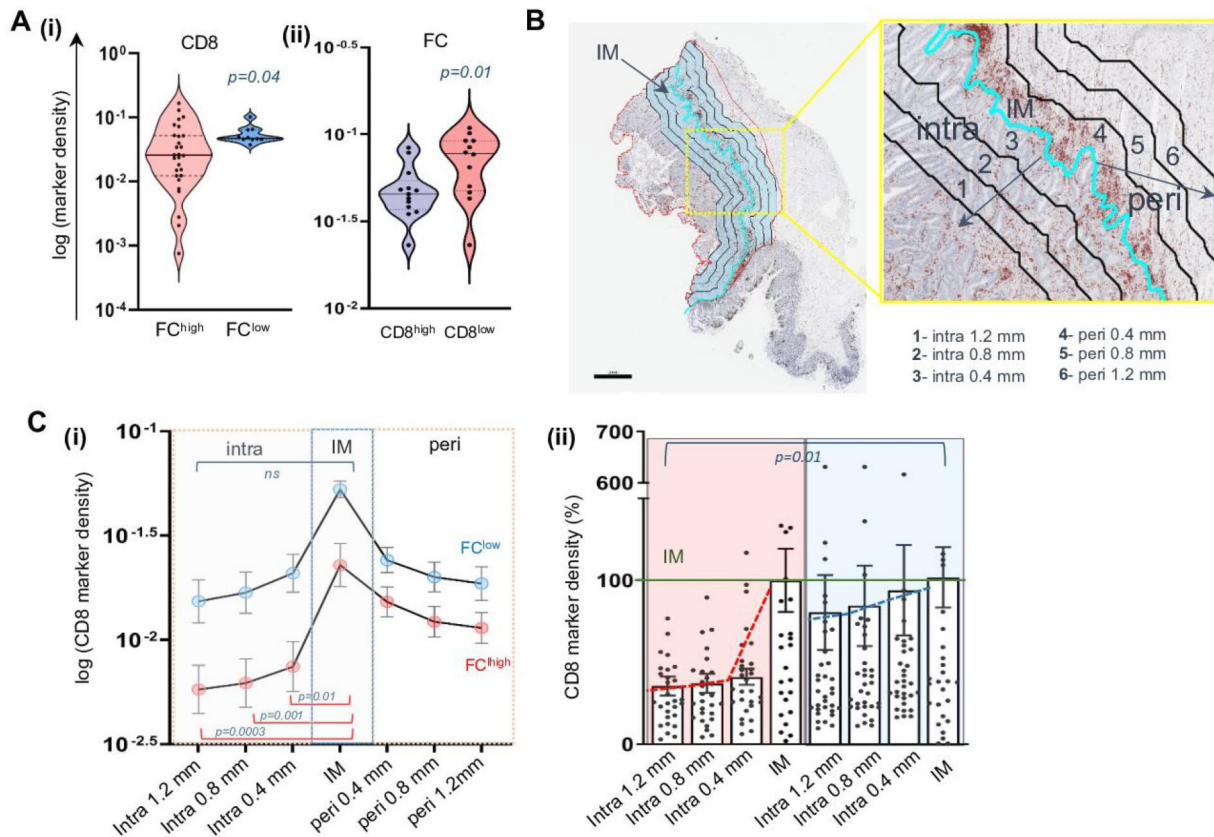


**Figure 2** CD8 spatial distribution with respect to foam cells (FC) presence. (A) Violin plot displaying (A(i)) CD8 and (A(ii)) FC accumulation with respect to FC and CD8 quantification, respectively; (B) representative image of the regions of interest segmented in the whole slide colorectal cancer (CRC) tissue section within 1.2 mm intra- and peri-tumoral to the invasive margin (IM); (C(i)) curves representing spatial distribution of CD8 T infiltrate in  $FC^{high}$  and  $FC^{low}$ ; (C(ii)) CD8 T infiltrate in the different intracellular localizations was expressed in % with respect of total CD8 at IM, accounted as 100%. Statistic by two-tailed Mann Whitney U-test (and two-way analysis of variance).

The quantification of CD8 gradient from peri-tumoral (peri) to intra-tumoral (intra) localization by applying a 400  $\mu$ m width intervals (figure 2B) showed that in  $FC^{high}$  tumors,  $CD8^+$  T cells progressively declined from the lesion edge towards the internal localization, with the marker density decreasing to  $0.017 (\pm 0.004; p=0.01)$ ,  $0.014 (\pm 0.003; p=0.001)$ , and  $0.013 (\pm 0.003; p=0.0003)$  at 0.4, 0.8, and 1.2 mm, respectively. Contrarily, the CD8 quantification was not significantly modulated with regards to the IM in  $FC^{low}$  cancer (figure 2C(i)). Globally, only 35% of the CD8 infiltrate present in the IM could reach the TC (1.2 mm) in  $FC^{high}$  with respect to the 80% of the  $FC^{low}$  setting (figure 2C(ii)). Summarizing, this detailed special analysis showed that the disparity in CD8 intratumor infiltrate detected in our CRC case set is strictly influenced by FC abundance at the IM, indicating a potential role of these cells in restraining the influx of T-cell effectors deep into the TME.

### FC-wall assumes a clinical significance in stage I–III CRC

The impact of the FC versus  $CD8^+$  T cells interplay on disease-free survival (DFS) was evaluated using Kaplan-Meier analyses. First, to elucidate the reciprocal impact of FC and  $CD8^+$  T cells on DFS, patients with a high versus low FC/CD8 ratio (cut-off 2.6) were compared.

Patients with high FC/CD8 ratio exhibited a significant poor DFS (log-rank  $p=0.002$  (online supplemental figure S3A)). Subsequently, Kaplan-Meier curves were applied separately to assess this impact in poorly and highly immunogenic tumors. CRC with high  $CD8^+$  cells in IM (cut-off 0.025) showed a 3-year DFS rate of 63.6% versus 20.8% in  $CD8^{low}$  CRC (log-rank  $p=0.009$ ) (figure 3A). However, within the  $CD8^{low}$  patients, the presence of the  $FC^{high}$  phenotype (cut-off 0.02) was associated with a significantly lower 3-year DFS rate (8.6%) compared with  $FC^{low}$  cases, which showed a 28.7% 3-year DFS (log-rank  $p=0.001$ ) (figure 3A). In contrast, no prognostic difference was observed between low and high non-FC density at IM (cut-off 0.107) in  $CD8^{low}$  CRC (log-rank  $p=0.19$  (online supplemental figure S3B)), nor between  $FC^{high}$  and  $FC^{low}$  density in  $CD8^{high}$  patients (log-rank  $p=0.17$  (online supplemental figure S3C)). This likely suggests that in the  $CD8^{high}$  group, the density of FC was not sufficient to counteract the antitumor activity of effector  $CD8^+$  T-cells, which is associated with improved survival.

Clustering patients by the presence ( $n=33$ ) or absence ( $n=32$ ) of recurrence at 3-year follow-up showed a notable enrichment of  $FC^{high} CD8^{low}$  and general reduction of

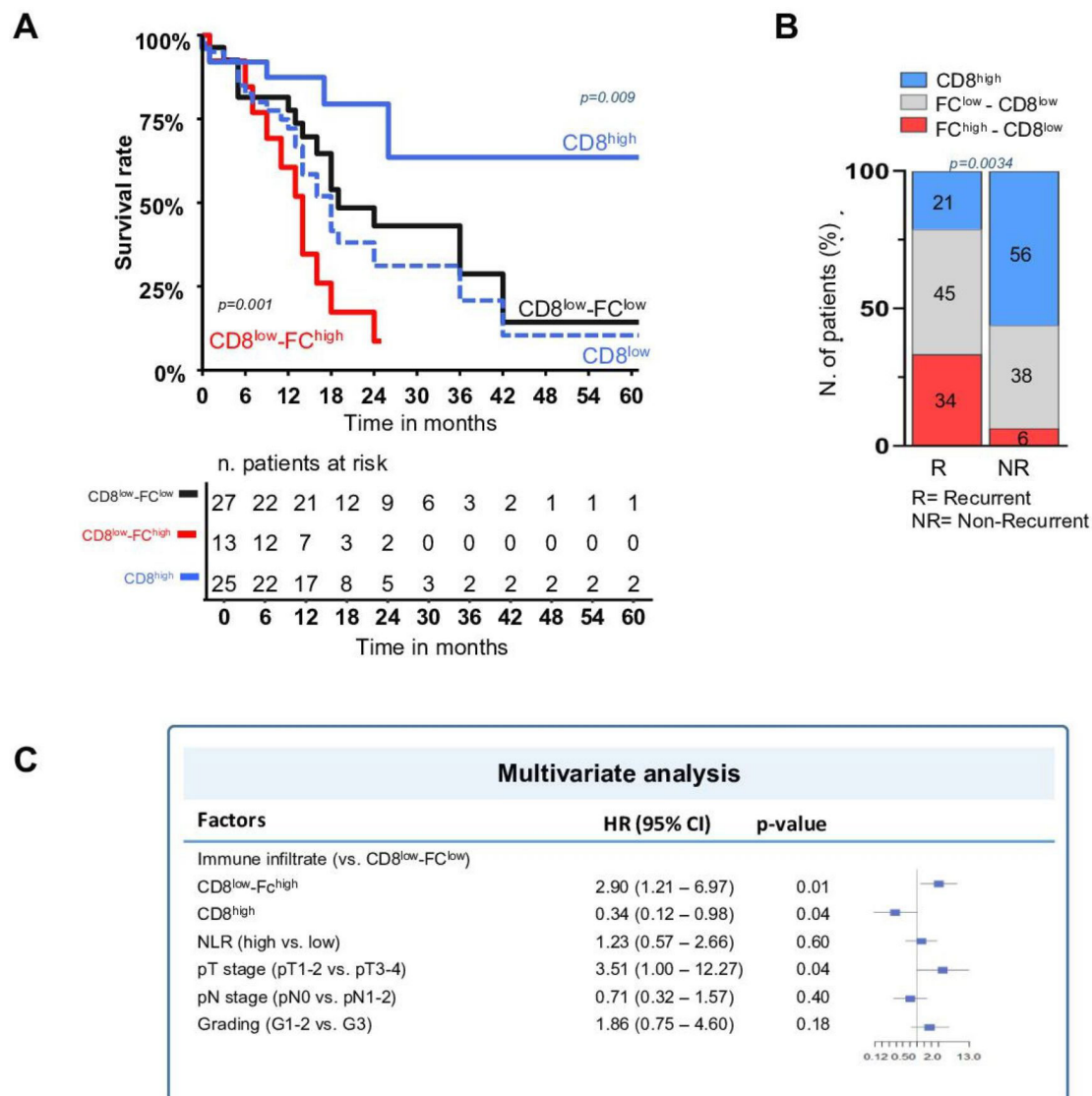


**Figure 3** Foam cells (FC) quantification identifies a subset of poorly immunogenic colorectal cancer with worse disease outcome. (A) Kaplan-Meier curves and number of patients at risk for disease-free survival (DFS) with CD8<sup>high</sup>, CD8<sup>low</sup>, FC<sup>low</sup> CD8<sup>low</sup>, and FC<sup>high</sup> CD8<sup>low</sup>. Log-rank p values from Mantel-Cox test are indicated; (B) stacked graph representing % of patients with recurrent (R) and non-recurrent (NR) disease according to the type of immune infiltrate at the invasive margin.  $\chi^2$  test for statistic; (C) multivariate analysis and forest plot of clinical and immune infiltrate profile associated with DFS. P values are determined by Cox proportional regression model.

CD8<sup>high</sup> cases within the recurrent population compared with disease-free patients (figure 3B).

Univariate Cox regression analysis indicated that FC<sup>high</sup> CD8<sup>low</sup> phenotype was one of the strongest negative prognostic factors associated with DFS (HR 2.47;  $p=0.02$ ), together with CEA (HR 1.14;  $p=0.002$ ), Ca19.9 (HR 1.57;  $p=0.004$ ), neutrophil-to-lymphocyte ratio (HR 1.13;  $p=0.025$ ), extramural vascular invasion (HR 2.55;  $p=0.01$ ), and perineural invasion (HR 2.12;  $p=0.038$ ). In contrast, CD8<sup>high</sup> phenotype showed a potent protective effect (HR 0.29;  $p=0.01$ ) (online supplemental table S7), in line with the validated role of the Immunoscore.<sup>4</sup> On multivariate Cox analysis, the only independent factors associated with DFS were pT stage (HR 3.5;  $p=0.04$ ), FC<sup>high</sup> CD8<sup>low</sup> (HR 2.9;  $p=0.01$ ), and the

CD8<sup>high</sup> cells (HR 0.33;  $p=0.04$ ). Harrell's C-index was 0.66 (figure 3C).

These findings confirm the clinical relevance of the immunosuppressive features of FC, and these cells significantly impact on disease progression when protective CD8-mediated immunosurveillance is lacking.

#### Tissue FC associated with distinct intratumoral immune cell contexture

Multiparametric flow cytometry analysis performed on fresh single cell suspension from tumor lesions of our CRC case set ( $n=21$ ) depicted an overall enrichment of CD14<sup>+</sup> ( $4.9\pm 4.3$  vs  $0.98\pm 1$ ;  $p=0.0001$ ) and CD4<sup>+</sup> T cells ( $39.2\pm 15.1$  vs  $14.3\pm 7.7$ ;  $p<0.0001$ ) paired with reduced



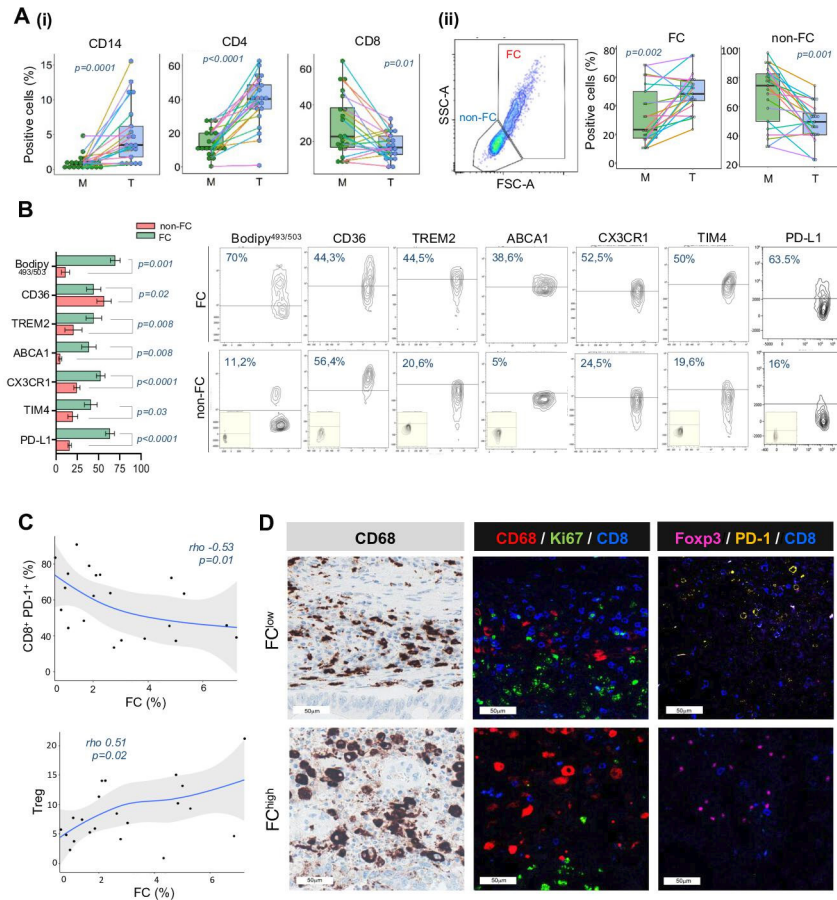


**Figure 4** Stage I-III colorectal cancer immunoprofile in relation to the presence of FC<sup>high</sup> and FC<sup>low</sup> infiltrate. Frequency of (A(i)) CD14<sup>+</sup>, CD8<sup>+</sup>, and CD4<sup>+</sup> T cells in tumor (T) and distant unaffected mucosa (M), and (A(ii)) representative flow cytometry plots showing physical parameters (forward and side scatter-area, FSC-A and SSC-A) of non-foam cells (FC) and FC CD14<sup>+</sup> with boxplots relative to their distribution in T and M; (B) histograms and dotplots of the % of positive cells for the indicated markers among FC and non-FC in tumor sample; p values are determined by Wilcoxon signed-rank test (n=21); (C) regression plots between infiltration FC and activated subsets (PD1<sup>+</sup>CD8<sup>+</sup>) or regulatory T cells (Tregs) (CD4<sup>+</sup>CD25<sup>hi</sup>CD127<sup>-</sup>) in tumors. P value and r coefficient are determined by Spearman correlation; (D) representative images of CD68-immunostained FC<sup>high</sup> and FC<sup>low</sup> CRC and confocal microscopy of CD68, Ki67, CD8 (red, green, and blue, respectively) and Foxp3, PD-1, CD8 (pink, yellow, and blue, respectively) matrix panels.

CD8<sup>+</sup> (17.5±7.3 vs 28.5±16.8; p=0.01), compared with patient-matched unaffected mucosa (figure 4A(i)).

As expected, the whole immune context of the tumor lesion was remarkably different from that of the corresponding normal colon mucosa (online supplemental figure S4), with immunosuppressive and regulatory populations being enriched along with reduced antitumor immune effectors. Indeed, CRC displayed enhanced infiltrate of the monocytic MDSC (CD14<sup>+</sup> HLA-DR<sup>-</sup>) (17.7±19.1 vs 9±10.9; p=0.004) and reduced frequency of CX3CR1<sup>+</sup> CD14<sup>+</sup> cells (39.5±25 vs 53.4±33; p=0.02), which are associated with resident macrophages in steady-state colon.<sup>25</sup> Within T-subsets, activated PD-1<sup>+</sup> (49.7±21 vs 29±22.4; p=0.003) and regulatory HLA-DR<sup>+</sup> (40.3±21.7 vs 17.7±14.5; p=0.004) CD8<sup>+</sup> T-cells were expanded in tumors, while the resident memory CX3CR1<sup>+</sup> CD8<sup>+</sup> T-cells<sup>26</sup> significantly declined (4.9±4.1 vs 8.4±8; p=0.02). CRC specimens were also characterized by increased frequency of regulatory CD4<sup>+</sup>CD25<sup>hi</sup>CD127<sup>-</sup> T cells (Tregs) (20.7±8 vs 9±6.1; p=0.0004) and CCR4<sup>+</sup> effector Treg (21.2±18.3

vs 15±14.8; p=0.004), along with a contraction of Th1 CD4<sup>+</sup>CX3CR3<sup>+</sup> (9.2±10.4 vs 25.4±15.2; p<0.0001) T cell subsets (online supplemental figures S4 and S5). We also detected FC within the tumor-infiltrating CD14<sup>+</sup> myeloid population based on the larger morphology and the higher structural complexity with respect to the non-FC counterpart. Remarkably, FC were significantly more abundant in tumor specimens compared with matched distant mucosa (49.29±13.22 and 32.67±21.10, respectively; p=0.002), while non-FC were significantly accumulated in mucosa (68.09±20.67) compared with tumor (49.16±13.00; p=0.001) (figure 4A(ii)).

The results obtained from multiparametric flow cytometry revealed that FC were characterized by the expression of distinct metabolic and functional markers associated with the induction of tumor immune tolerance. The modulation of these markers differed significantly compared with their non-FC counterparts (figure 4B). Specifically, Bodipy<sup>493/503</sup> staining, indicating cellular lipid content, was expressed in 70% of FC, compared with

only in 11.1% of non-FC ( $p=0.001$ ). Mirroring their active lipid metabolism, FC exhibited modulated expression of lipid transporter proteins, including upregulation of TREM2 (44.5%;  $p=0.008$ ) and ABCA1 (38.6%;  $p=0.008$ ), and downmodulation of CD36 (44.3%;  $p=0.02$ ), in comparison with their non-FC counterpart (20.6%, 4.9%, and 58.4%, respectively) (figure 4B). Additionally, FC showed significantly higher expression of the phosphatidylserine (PS) receptor Tim4 (40.9%;  $p=0.03$ ), the chemokine receptor CX3CR1 (52.5%;  $p<0.0001$ ) and the inhibitory immune checkpoint PD-L1 (63.5%;  $p<0.0001$ ) compared with non-FC (19.6%, 24.5%, and 16%, respectively) (figure 4B), defining features of long-lived resident macrophages<sup>27</sup> with a potential role in impairing anti-tumor T cell response and inducing regulatory subsets.<sup>28</sup> Along with the increased expression of the myeloid lineage markers CD68 and CD163, FC notably exhibited higher expression of CD206 (80.7%;  $p=0.06$ ) and PD-L1 (compared with the non-FC, as an additional immunosuppressive pathway to blunt antitumor immunity (online supplemental figure S6). Notably, the abundance of FC was found to negatively correlate with the presence of activated CD8<sup>+</sup>PD-1<sup>+</sup> effector subsets ( $p=0.01$ ), while it was positively associated with Tregs ( $p=0.02$ ) (figure 4C). In contrast, no correlation between non-FC and effector or regulatory T cell subsets was observed (online supplemental figure S7). In summary, the immunological hallmarks of FC-enriched CRC indicate a tolerogenic and pro-tumor environment, characterized by the exclusion of activated CD8<sup>+</sup> T cells and the predominance of Tregs. This observation was also supported by confocal analyses, revealing lack of the PD-1 activation marker in CD8<sup>+</sup> T cells, decreased total CD8<sup>+</sup> T cell infiltration, and increased presence of FoxP3<sup>+</sup> Tregs in FC<sup>high</sup> tumors. Furthermore, CD8<sup>+</sup> T cells in FC<sup>high</sup> CRC did not colocalize with the proliferative marker Ki67 (figure 4D), thus revealing poor proliferative potential.

### Transcriptional profile of FC-enriched CRC is compatible with a multimodal dampening of tumor immunosurveillance

TGF- $\beta$  is an acknowledged player of the immunosuppressive activity mediated by FC in chronic inflammatory setting such as atherosclerosis,<sup>29</sup> and a key immune escape mediator in TME.<sup>30</sup> Hence, our subsequent objective was to assess whether TGF- $\beta$  could be linked to the restrained T-cell immunity associated with FC. IM CRC regions with an average area of 0.05 mm<sup>2</sup> were analyzed by IF. The FC<sup>high</sup> area, marked by a substantial accumulation of Bodipy<sup>+</sup> and CD68<sup>+</sup> FC, was compared with matched FC<sup>low</sup> area, where the average FC accumulation was 80% vs. 32% (figure 5A). The FC<sup>high</sup> area exhibited a twofold higher TGF- $\beta$  level compared with the FC<sup>low</sup> area (13% vs 5.7%;  $p=0.007$ ) (figure 5A). Furthermore, TGF- $\beta$  was found to be independently associated with FC compared with non-FC elements across different observed areas, reaching statistical significance particularly in FC<sup>high</sup> area ( $p=0.02$ ) (figure 5B).

Our next step was to functionally characterize FC immune suppressive features by assessing the transcriptional profile of FC<sup>high</sup> and FC<sup>low</sup> CRC, selected from the digital pathology quantification (online supplemental table S5A).

Analyses from bulk RNAseq data revealed 2900 differentially expressed (DE) genes (FDR<0.05) from FC<sup>high</sup> and FC<sup>low</sup> CRC tissue specimens (online supplemental figure S8A and table S5B). Specific FC-associated transcriptomic programs were identified by crossing the expression levels with cell-state specific genes listed in micro-dissected FC-enriched and deprived tumors.<sup>31</sup> 881 genes with coherent differential expression were identified (online supplemental figure S8B and table S5B). Specifically, 676 genes were upregulated, whereas 205 were downregulated in FC<sup>high</sup> CRC in both studies (FDR<0.05). Unsupervised enrichment analyses based on upregulated and downregulated coherently modulated genes (online supplemental table S5C) revealed a scenario resembling a state of immune hyporeactivity in FC<sup>high</sup> CRC. Selected terms from the Reactome Gene Set and GO Biological Processes (figure 5C, online supplemental table S5D), showed upregulation of negative type I interferon production and innate immune response as detected by the genes *RNF125*, *HAVCR2*, *NLRC3*, *PTPN2* and *CD96*, as well as, enhanced cell proliferation as depicted by the upregulation of “EGFR signaling pathway” and downregulation of “degradation of  $\beta$ -catenin.”

Additionally, FC<sup>high</sup> CRC showed significantly negative enrichment of a core set of genes implicated in class I-II MHC mediated antigen presentation and processing, such as *AP2B1*, *ARF1*, *DYNCL12*, *KIF5B*, *DYNLL1*, *SEC24C*, *BLMH*, *TPP2*). Moreover, the term related to “downstream TCR signaling” was also significantly negative enriched (*PSMA4*, *AP2B1*, *ARF1*, *KIF3B*, *SEC24C*, *URB4*, *TUBA1B*), indicating that the functions and cross-talk between adaptive and innate immunity are inhibited in FC-enriched CRC.

Alongside the altered antitumor immunity, FC<sup>high</sup> CRC exhibited changes in lipid metabolism, indicated by the significant negative enrichment of the term “cholesterol biosynthesis process,” including downregulation of *ACLY*, *DHCR24*, *HMGCR*, *ID1L*, *EBP*, *NSDHL*, and *PLPP6* genes. Furthermore, this process was accompanied by mitochondrial dysfunction, as evidenced by the significant downmodulation of a core set of gene involved in mitochondrion organization and biosynthesis (*TIMM8A*, *HSPA4*, *NDUFA8*, *VDAC2*, *COA1*, *ACACA*, *ACAT1*, and *HMGCR*).

Next, we examined immune-related gene signatures in FC<sup>high</sup> and FC<sup>low</sup> CRC. The interferon gamma (IFN $\gamma$ ) activating signature (IFNG\_score\_21050467),<sup>32</sup> comprising genes associated with effective immunosurveillance and favorable prognosis in patients with cancer was found to be reduced in FC<sup>high</sup> CRC (figure 5D, online supplemental table S5E). Conversely, there was an increase in signature associated with T-cell exhaustion (inhibitory)<sup>32</sup> and Tregs<sup>26</sup> in FC<sup>high</sup> CRC. Additionally, compared with



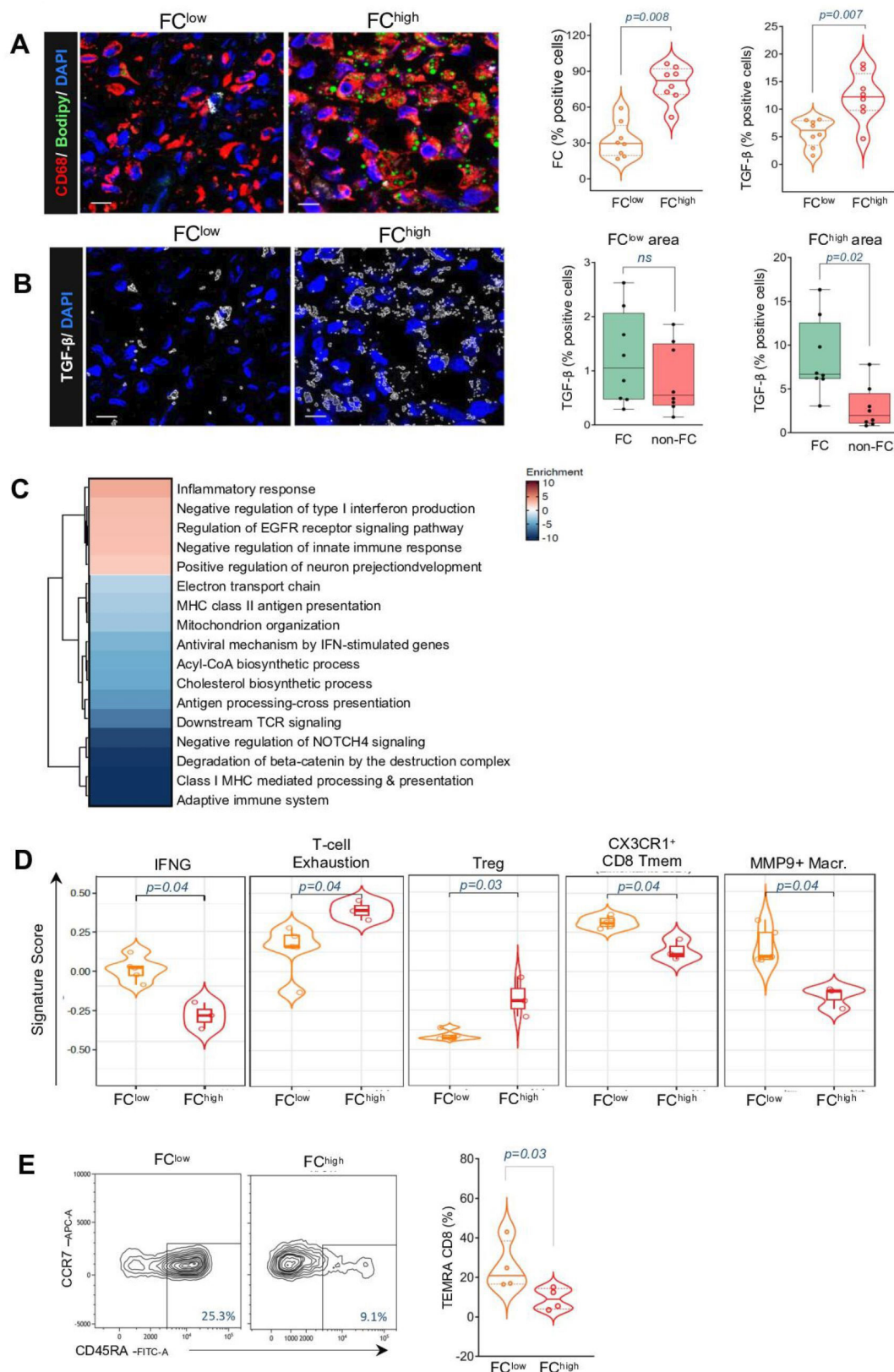


**Figure 5** Foam cells (FC) alter T-cell functional program at local levels of colorectal cancer (CRC). (A) Representative images of (A) CD68 (red) and Bodipy<sup>493/503</sup> (green), and (B) transforming growth factor-beta (TGF- $\beta$ ) (white) staining of  $FC^{high}$  and  $FC^{low}$  regions of CRC tissue and relative boxplots of marker expression; DAPI (blue) was used for the nuclei; (C) heatmap of the significant enrichment annotations of coherent DE genes between  $FC^{high}$  versus  $FC^{low}$  CRC of our study and those of micro-dissected FC-enriched CRC from Luca *et al* study; (D) immune-associated signature score in  $FC^{high}$  versus  $FC^{low}$  CRC. (E) %positive terminal effector cells (TEMRA) in  $FC^{high}$  and  $FC^{low}$  CRC. P values are calculated by Wilcoxon and Mann-Whitney test for dependent and independent observations, respectively; ns, not significant.

FC<sup>low</sup> tumors, transcriptional pathways indicative of memory CD8 (CX3CR1<sup>+</sup> CD8 Tmem) and various subsets of activated colonic macrophages (MMP9<sup>+</sup> inflammatory macrophage) were downregulated in FC<sup>high</sup> samples<sup>26</sup> (figure 5D, online supplemental table S5E). To validate the findings of the dysfunctional state of antitumor immunosurveillance in the presence of FC, tumor cell suspensions were assessed for abundance of differentiated effector cells. FC<sup>high</sup> CRC were characterized by lower proportion of terminally differentiated effector memory CD8<sup>+</sup> T cells (TEMRA) compared with FC<sup>low</sup> CRC (figure 5E). This suggests that weak T cell receptor engagement and limited immune response to tumor antigens may occur within the TME in the presence of lipid-engulfed macrophages.

Overall, these findings suggest that FC-enriched CRC are characterized by immunosuppressive milieu that, through the impaired CD8 T-cell proliferation and activity, accrual of regulatory CD4, and loss of homeostatic function in resident myeloid cells, leads to the complete subversion of local immunosurveillance.

#### TGF- $\beta$ targeting could restore the activation of effector T cell

To investigate the FC-associated immunosuppression, we exploited in vitro-generated human FC. Early macrophages, derived from CD14<sup>+</sup> isolated from PBMCs of HDs, were engulfed with oxLDL for 48 hours (figure 6A). To determine whether in vitro-generated FC accurately reflect the characteristic of in vivo lipid-engulfed macrophages, their transcriptional profiles were evaluated by bulk RNAseq (GSE273106 GEO identifier). Early macrophages treated with oxLDL showed 161 DE genes (FDR<0.05) compared with controls (online supplemental table S5F). Subsequently, DE genes of in vitro FC were then compared with those identified in vivo. A total of 429 DE genes in FC<sup>high</sup> versus FC<sup>low</sup> CRC were coherently DE with genes identified in micro-dissected FC-enriched tumors<sup>31</sup> and in vitro-derived FC. Enrichment analyses of these 429 DE genes revealed 338 significantly enriched terms outlining the overall functional state of FC (online supplemental table S5G). Among the 20 top enriched terms (online supplemental figure S9A), pathways related to lipid metabolism were notably modulated. Specifically, 40 coherently DE genes enriched the term “metabolism of steroids” (R-HSA- 8957322, FDR<0.001) were further investigated. Unsupervised hierarchic clustering of these genes across the in vitro and in vivo FC demonstrated similar gene modulation in lipid-engulfed macrophages, indicating that, despite potential differences in their biogenesis, in vitro FC closely resemble their in vivo counterparts (figure 6B). Consistent with the in vivo findings where FC<sup>high</sup> CRC tissue exhibited significantly higher TGF- $\beta$  staining compared with FC<sup>low</sup> tissue, in vitro-generated FC also produced significantly higher levels of TGF- $\beta$  (261 $\pm$ 97 vs 195 $\pm$ 68; p=0.03) compared with non-engulfed CD14<sup>+</sup> cells (figure 6C). This results underscores TGF- $\beta$ , as a potential key modulator in the FC-mediated inhibition of antitumor immunosurveillance,

supporting its role in the immune evasion mechanism observed in CRC.

To further bear the role of lipid-engulfed macrophages in promoting an immunosuppressive milieu within TME, in vitro-generated FC derived from both HD and CRC were thoroughly characterized by their phenotype. Overall, lipid engulfment resulted in comparable marker modulation in CD14<sup>+</sup> cells in both healthy and disease conditions, closely resembling the FC phenotype observed in CRC tissue (figure 6D). Specifically, the abundance of cells stained positive for Bodipy<sup>493/503</sup>, was significantly increased in oxLDL-treated early macrophages compared with controls (1.9% $\pm$ 1.6 vs 7.1 $\pm$ 4.5 in HD and 1.7% $\pm$ 0.7 vs 9% $\pm$ 5.2 in CRC; p=0.004). Mirroring tissue FC, in vitro lipid-loaded cells exhibited higher expression of ABCA1 transporter (23.8% $\pm$ 14.1 vs 58.5% $\pm$ 18.5 in HD and 9.1 $\pm$ 5 vs 47.9% $\pm$ 12.1 in CRC; p<0.001) and a reduction of the scavenger receptor CD36, as indicated by the enhancement of the CD36-negative fraction (15.3% $\pm$ 11.4 vs 43.2% $\pm$ 14.9 in HD and 5.3% $\pm$ 3.3 vs 29.5% $\pm$ 14.7 in CRC; p<0.0001). The chemokine receptor CX3CR1 was also increased in lipid engulfed macrophages compared with control (2.1% $\pm$ 0.9 vs 9.5% $\pm$ 7.5 in HD and 1.8% $\pm$ 1.5 vs 10.3% $\pm$ 6.1 in CRC; p<0.001). Similarly, the inhibitory immune check point PD-L1 was enhanced in FC counterparts (2.5% $\pm$ 1.3 vs 15.5% $\pm$ 11.8 in HD and 0.8% $\pm$ 0.7 vs 4.1% $\pm$ 3.5 in CRC, p=0.004).

Additional phenotypic features, such as the increase in CD163 marker expression and the decreased expression of the costimulatory molecule CD86 (online supplemental figure S9B), further support the lipid-associated polarization towards immunosuppressive myeloid cells.

To evaluate the mechanisms hindering effective CD8-T cell-mediated antitumor immunity associated with lipid engulfment in the CD14<sup>+</sup> population, TCR-stimulated autologous T cells were cocultured with in vitro-induced FC or control cells. A significantly reduced CD8<sup>+</sup> T-cell proliferation was detected by CFSE assay in FC-conditioned cultures compared with non-engulfed CD14<sup>+</sup> cells (28.3 $\pm$ 13.8 vs 43 $\pm$ 8.4; p=0.0005) (figure 6E (i)). We also assessed the frequency of CD25<sup>+</sup> subsets on proliferating CD8<sup>+</sup>, as an indicator of cell activation. We found that in FC coculture, the frequency of proliferating CD8 T-cells expressing CD25 marker was significantly lower compared with control condition (7 $\pm$ 5.1 vs 11.6 $\pm$ 5.1; p=0.001) (figure 6E (ii)). In parallel, the concentration of the cytotoxic factor, Granzyme B, was significantly lower in T-cell:FC cocultures compared with the control group (2.8 $\pm$ 2.7 vs 4.6 $\pm$ 4.7; p=0.004) (figure 6E (iii)).

Given the decrease in PD-1 positive T-cells in FC<sup>high</sup> tumor regions and the increased expression of PD-L1 in tissue and in vitro foamy macrophages, as well as the increased production of FC-associated TGF- $\beta$  immunosuppressive factor, we additionally conducted immunosuppression assays with the in vitro generated FC pretreated with single or simultaneously inhibition of TGF- $\beta$  and anti-PD-L1 signaling.

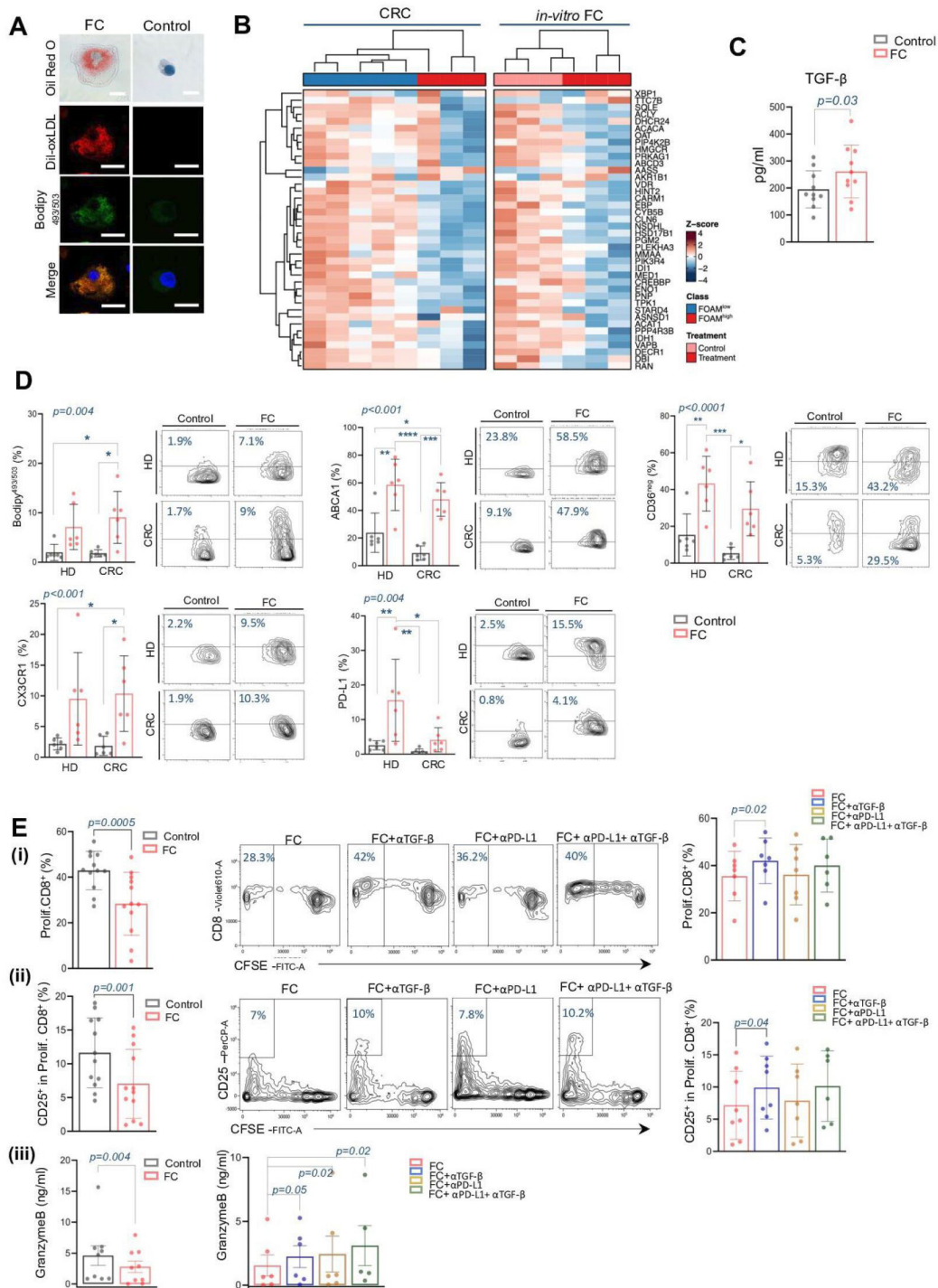


**Figure 6** Induced lipid-engulfed macrophages resemble tissue foam cells (FC) and reconstitute T cell dysfunctions. (A) Representative confocal image of the generated human FC model; (B) heatmap and z-score of gene enriched for metabolism of lipids in coherently differentially expressed genes between in vitro-generated FC and in vivo setting. (C) Transforming growth factor-beta (TGF- $\beta$ ) secretion in in-vitro derived FC compared with non-engulfed early macrophages (control); p value determined by Wilcoxon test. (D) Boxplots and representative dot plots with the mean values of the % of positive cells for the indicated markers in in vitro derived FC compared with controls in healthy donor (HD) and patients with colorectal cancer (CRC) (n=6). P values determined by two-way analysis of variance and Tukey's multiple comparison; (E) boxplots of the (i) proliferating and (ii) activated CD25<sup>+</sup> CD8<sup>+</sup> subsets, as well as, (iii) Granzyme B concentration in supernatants of control:T-cells and FC:T-cells cocultures at ratio 1:1 after 5 days of cocultures. The proliferation detected by CFSE dye dilution, activated CD25<sup>+</sup> subset and Granzyme B concentration were assed with or without prior FC pretreatment with or without single or simultaneously anti-TGF- $\beta$ 1,2,3 and anti-PD-L1 mAbs. Statistic was determined by Friedman test; showed p value referred to Dunn's post-hoc test (n=6-12).



TGF- $\beta$  blocking in human-derived FC, significantly restored the proliferation of CD8<sup>+</sup> T-cells ( $42\pm 9.7$  vs  $28.3\pm 13.7$ ;  $p=0.02$ ) (figure 6E(i)), and significantly enhanced the activation of proliferating CD8<sup>+</sup> ( $13\%\pm 6.6$  vs  $7\%\pm 5.1$ ;  $p=0.04$ ) (figure 6E(ii)), compared with T-cell:FC condition.

The anti-PD-L1 blockade did not enhanced CD8<sup>+</sup> T-cells proliferation ( $36.2\%\pm 12.8$ ) and nor increase the frequency of CD25<sup>+</sup> CD8<sup>+</sup> cells ( $7.9\%\pm 5.7$ ) in coculture with FC (figure 6E(i,ii)). However, the dual blockade of TGF- $\beta$  and PD-L1 did not restore inhibition of CD8 T-cell proliferation, suggesting that the inhibition is likely due only to TGF- $\beta$ , while PD-L1 is probably not involved (figure 6E(i,ii)). Notably, neither inhibitory treatment did not enhance the proliferation or activation of TCR-stimulated T-cells cultured alone (online supplemental figure S10A). This suggests that the activity of effector T-cells was dependent on inhibitory factors secreted by dyslipidemic macrophages.

The modulation of T-cell effector function in presence of FC, with singular or simultaneously TGF- $\beta$  and PD-L1 inhibition, was confirmed by quantifying released cytotoxic factors. In this case, the ability to produce Granzyme by T-cells was significantly restored in both single TGF- $\beta$  and PD-L1 blocking (figure 6E(iii)). However, their dual inhibition enhanced by twofold increase in Granzyme B production compared with T-cell:FC condition ( $3.1\pm 3.5$  vs  $1.5\pm 2$ ;  $p=0.02$ ) (figure 6(iii)), suggesting that FC-associated TGF- $\beta$  signaling could be able to alter the anti-PD-L1 cell response, in line with recent findings.<sup>33 34</sup> Single or simultaneously TGF- $\beta$  and PD-L1 blocking did not show any modulation in T-cell:non-engulfed macrophages cocultured (online supplemental figure S10A,B).

These data collectively highlight the role of FC-secreted TGF- $\beta$  as a critical factor in impeding protective CD8 anti-tumor immunity and underscore a potential targetable pathway for restoring effective T cell function.

## CONCLUSIONS

Primary CRC is a human malignancy in which local immunity, estimated by the quantification and spatial distribution of CD8<sup>+</sup> T cells, acts as a positive prognostic factor and the best predictor of DFS, more efficiently than the tumor-node-metastasis staging.<sup>35</sup> This strong adaptive immune response is believed to reflect the rich T cell neoantigen repertoire expressed by CRC tumors as a consequence of specific genetic profiles (eg, MSI-H/dMMR).<sup>36</sup> However, a high Immunoscore is detectable in merely 30% of CRCs,<sup>4</sup> while tumor DNA alterations potentially leading to T cell epitopes, but showing limited evidence of T cell infiltration, are found in a vast majority of cases.<sup>37</sup> These observations indicate that additional immune components of the CRC TME might be involved in hindering tumor T cell immunogenicity, and may deserve investigations for implementing immune-mediated control of this disease.

Several attempts have been made to identify myeloid subsets that correlate with CRC progression, including the proportion of CD163 or CD206 positive subpopulation on the CD68 pan-macrophages marker.<sup>38</sup> However, the identification of detrimental subsets could be very challenging, considering their ontogenically heterogeneous nature and above all their high plasticity.<sup>27 39</sup> Indeed, by rescuing catabolites imbalance within the TME, such as tumor secreted-lipids, macrophages rewired their metabolism and reshuffle their lipid composition<sup>40</sup> and phenotype, thus representing an appealing immunosuppressive mediator.<sup>41</sup>

This study provides valuable insights into the complex interplay between altered lipid metabolism, colonic macrophages and T-cell immunity in the context of stage I–III CRC, shedding the light on their collective impact on disease progression.

Given the recently findings on the association of lipid-engulfed macrophages in controlling metabolic disorders,<sup>42</sup> we have first demonstrated that FC, characterized by their lipid-laden phenotype, are associated with patients' BMI and specific systemic lipid composition, suggesting for the first time their linking role between obesity and CRC. Specifically, FC associated with increased palmitic and oleic acids and decreased omega-3 PUFA, despite the lack of macroscopic clinical dyslipidemia. In this regard, dietary palmitic acid has recently been associated with metastatic potential in oral carcinomas,<sup>43</sup> and it is well known that the unbalanced ratio between saturated and unsaturated lipids in membrane phospholipids could alter membrane fluidity and affect effector functions such as phagocytosis.

Then we have elucidated the significant role of FC in creating an immunosuppressive microenvironment within the colon, potentially fostering an immune milieu fueling tumor growth and progression. Specifically, FC identify CRC cases with a higher risk of recurrence after radical resection in patients with low immunogenic tumors. Indeed, the quantification of FC allowed for the identification of a subset of patients with CRC with a CD8<sup>low</sup> FC<sup>high</sup> phenotype, who displayed the shortest DFS with respect to patients with CD8<sup>low</sup> FC<sup>low</sup> and obviously with CD8<sup>high</sup> tumors. Interestingly, considering the balance of FC and CD8, 2.6-fold higher abundance of FC on CD8 is predictive of worse DFS, demonstrating that the burden of FC is relevant even in patients with presence of CD8 infiltrate.

In this context, FC are paired with a specific immune context, consisting of reduced CD8<sup>+</sup>PD1<sup>+</sup> T cells and enriched CD4<sup>+</sup> Treg and infiltration, which indicates an active role of FC in promoting local immune tolerance. Interestingly, this scenario is highly reminiscent of the FC described in atherosclerotic plaques, where they have been proven to actively induce Treg accrual and concomitant inhibition of pathogenic CD8<sup>+</sup> T cell effectors, resulting in plaque stabilization through the onset of an immunosuppressive milieu.<sup>44</sup> The MiaQuant digital pathology algorithm<sup>23 24</sup> allowed us to capture

FC within the entire macrophage population based on their specific morphology and size characteristics. Analysis of the spatial distribution of FC with respect to CD8<sup>+</sup> T cells in CRC lesions revealed a distinctive behavior of cancer-associated FC. The “barrier-like” distribution of FC controls the immune cells entering the neoplastic nests from the AM. High FC frequency at the CRC IM was thus confirmed to be associated with a significant decrease in the frequency of inner CD8 T cells, a correlation that was not detected when non-FC macrophages were evaluated. In line with this evidence, Peranzoni *et al* recently demonstrated the ability of macrophages to interfere with CD8 T cell motility and prevent them reaching tumor regions in lung squamous cell carcinoma.<sup>45</sup> We further reinforced the potential immunosuppressive activity of CRC-associated FC by reporting that CRC features of FC<sup>high</sup> infiltrate displayed enhanced dysregulation of TGF- $\beta$  signaling, potentially contributing to immune evasion and disease progression. The transcriptional program showed reduced expression of genes associated with IFN $\gamma$ -related pathways<sup>32</sup> and CD8 T memory cells,<sup>26</sup> while showing enrichment in terms related to Treg<sup>26</sup> and T cell exhaustion.<sup>32</sup> Furthermore, the presence of terminally differentiated effectors alongside FC delineates an impaired antitumor immunosurveillance.

Additionally, multiparametric flow cytometry analysis of CRC cell revealed a more complex dysfunctional immune environment coexisting with FC accumulation. To the already mentioned reduced frequency of CD8<sup>+</sup>PD1<sup>+</sup> activated T cells and the increased effector Treg accrual,<sup>46</sup> FC<sup>high</sup> tumors were thus found characterized by a loss of predominance of immunoregulatory cellular elements, including an increase of regulatory CD8<sup>+</sup>HLA-DR<sup>+</sup> subset<sup>47</sup> together with a decrease in CD4<sup>+</sup>CXCR3<sup>+</sup>, which underlies the impairment of the generation of Th1 effector.<sup>48</sup>

Notably, a remarkable decrease in CX3CR1 expression in myeloid and lymphoid components was detected in FC<sup>high</sup> tumors. CX3CR1 and its ligand, CX3CL1 (fractalkine), are pillar mediators of inflammation and autoimmune diseases.<sup>49</sup> When expressed in macrophages of the colonic lamina propria, the CX3CR1/CX3CL1 axis mediates T cells activation leading to colitis,<sup>50</sup> indicating a key role for this pathway in the accrual of intestinal T-cell effectors and suggesting its loss as a potential mechanism of immune escape in CRC.

Further, our investigation delves into the intricate interplay between FC and the potential interventions to restore effective antitumor immunosurveillance. TGF- $\beta$  emerges as a promising therapeutic strategy to disrupt FC-mediated immunosuppression, potentially restoring effective antitumor immunity.

Additionally, TGF- $\beta$  inhibition was found to enhance the ability of anti-PD-L1 in restoring T-cell activity. This aligns with recent preclinical studies showing that simultaneous targeting of both pathways enhances tumor infiltrating T-cell in tumors with a CD8 desert phenotype.<sup>33,34</sup>

The present study has some limitations. First, the sample size of accrued patients is relatively small, which may limit the ability to fully verify the strength of FC as a negative prognostic biomarker, particularly in CD8<sup>high</sup> CRC cases. Additionally, the FC model established here represents a simplified version compared with the *in vivo* FC, which arise from chronic exposure of TME macrophages to local and systemic modulating factors. These *in vivo* FC may secrete other inhibitory factors that could be involved in the suppression of CD8 effector activity. Furthermore, conducting immunosuppression assays by stimulating T cells with tumor antigens, which more closely mimic the physiological TME, could reflect a more realistic condition and potentially results in even greater observed immunosuppression.

In conclusion, our study showed that FC<sup>high</sup> CD8<sup>low</sup> CRC, representing 20% of patients, have the highest risk of recurrence after radical surgery, suggesting the possibility of implementing Immunoscore with FC quantification to identify patients who may have worse clinical outcomes. Additionally, this study sheds light on the critical role of lipid-laden macrophages in mediating immune modulation in CRC pathogenesis, providing a novel avenue for therapeutic intervention in CD8 T-cell excluded patients. This offers a promising opportunity to improve therapeutic outcomes and patient survival in CRC. Finally, the link observed between FC tissue accrual, BMI and specific lipid profiles in patient plasma supports the use of interventions targeting lipid metabolism as a complementary approach to enhance effective tumor immunosurveillance by interfering with macrophage lipid metabolism in CRC treatment and prevention.

#### Author affiliations

<sup>1</sup>Unit of Translational Immunology, Department of Experimental Oncology, Fondazione IRCCS, Istituto Nazionale dei Tumori di Milano, Milan, Italy

<sup>2</sup>School of Medicine and Surgery, University of Milano Bicocca, Monza, Italy

<sup>3</sup>Department of Clinical and Biological Sciences, University of Turin, Turin, Italy

<sup>4</sup>Anacleto Lab, Computer Science Department, University of Milan, Milan, Italy

<sup>5</sup>Molecular Epigenomics, Department of Research, Fondazione IRCCS Istituto Nazionale dei Tumori, Milan, Italy

<sup>6</sup>Research in Nutrition and Metabolomics, Department of Research, Fondazione IRCCS Istituto Nazionale dei Tumori di Milano, Milan, Italy

<sup>7</sup>Candiolo Cancer Institute, FPO-IRCCS, Candiolo, Turin, Italy

<sup>8</sup>IIGM-Italian Institute for Genomic Medicine, c/o IRCCS, Candiolo, Turin, Italy

<sup>9</sup>Laboratory Medicine Division, Fondazione IRCCS Istituto Nazionale dei Tumori, Milan, Italy

<sup>10</sup>Immunohematology and Trasfusion Medicine Service (SIMT), Fondazione IRCCS Istituto Nazionale dei Tumori, Milan, Italy

<sup>11</sup>Unit of Hereditary Digestive Tract Tumors, Department of Surgery, Fondazione IRCCS Istituto Nazionale dei Tumori, Milan, Italy

<sup>12</sup>Department of Pharmacological and Biomolecular Sciences, University of Milan, Milan, Italy

<sup>13</sup>First Division of Pathology, Department of Pathology and Laboratory Medicine, Fondazione IRCCS Istituto Nazionale dei Tumori, Milan, Italy

<sup>14</sup>Unit of Colorectal Surgery, Department of Surgery, Fondazione IRCCS Istituto Nazionale dei Tumori, Milan, Italy

**Acknowledgements** Graphical abstract was created with “BioRender.com”.

**Contributors** ED—conceptualization: lead; investigation: lead; data curation: equal; supervision: lead; writing-original draft: lead; guarantor; BV—investigation: equal; visualization: equal; LL—formal analysis: equal; visualization: equal;

GF—investigation: equal; formal analysis: equal; visualization: equal; writing—original draft: supporting; EC—investigation: equal; methodology: lead; software: lead; writing—original draft: supporting; AC—investigation: equal; data curation: equal; visualization: equal; MZ—investigation: equal; VH—investigation: equal; writing—review and editing: equal; MG—investigation: supporting; writing—review and editing: equal; PP—investigation: equal; resources: equal; SG—investigation: equal; resources: equal; DM—investigation: equal; FA—investigation: equal; MV—resources: equal; investigation: equal; PAC—investigation: equal; resources: equal; conceptualization: supporting; AMR—data curation: equal; MS—data curation: supporting; investigation: equal; PF—data curation: supporting; investigation: equal; VL—investigation: equal; data curation: equal; LC—investigation: equal; data curation: equal; GS—data curation: equal; MC—resources: equal; investigation: equal; BEL—resources: equal; investigation: equal; writing—original draft: equal; MM—resources: equal; investigation: equal; LS—conceptualization: lead; investigation: lead; resources: equal; writing—original draft: equal; LR—conceptualization: lead; investigation: lead; resources: lead; writing—original draft: lead; project administration: lead. LS and LR are joint last authors.

**Funding** This work was funded by AIRC Project IG 2017 Id.20752. The research leading to these results has received funding from AIRC under IG 2022 - ID. 27841 project to RL (PI). This work was supported in part by 5 X 10005 Funds—2014 MIUR—to MV. ED was supported as postdoctoral fellow by Umberto Veronesi Foundation for the year 2022–2024 and Pezcoller-SIC Foundation for the year 2021.

**Competing interests** None declared.

**Patient consent for publication** Consent obtained directly from patient(s).

**Ethics approval** This study involves human participants and was approved by Ethics Committee of the Fondazione IRCCS, Istituto Nazionale dei Tumori, Milan (INT), Italy (INT127/19, INT149/19, INT61/20). Informed consent was obtained from all patients and HDs.

**Provenance and peer review** Not commissioned; externally peer reviewed.

**Data availability statement** Data are available upon reasonable request. Data are available upon reasonable request. All data associated with this study and its supplementary data files are available within the article. Sequencing and bioinformatics analyses were annotated in Gene Expression Omnibus Super Series: GSE227206 and GSE273106.

**Supplemental material** This content has been supplied by the author(s). It has not been vetted by BMJ Publishing Group Limited (BMJ) and may not have been peer-reviewed. Any opinions or recommendations discussed are solely those of the author(s) and are not endorsed by BMJ. BMJ disclaims all liability and responsibility arising from any reliance placed on the content. Where the content includes any translated material, BMJ does not warrant the accuracy and reliability of the translations (including but not limited to local regulations, clinical guidelines, terminology, drug names and drug dosages), and is not responsible for any error and/or omissions arising from translation and adaptation or otherwise.

**Open access** This is an open access article distributed in accordance with the Creative Commons Attribution Non Commercial (CC BY-NC 4.0) license, which permits others to distribute, remix, adapt, build upon this work non-commercially, and license their derivative works on different terms, provided the original work is properly cited, appropriate credit is given, any changes made indicated, and the use is non-commercial. See <http://creativecommons.org/licenses/by-nc/4.0/>.

#### ORCID iDs

Elena Daveri <http://orcid.org/0000-0001-8351-2762>  
 Elena Casiraghi <http://orcid.org/0000-0003-2024-7572>  
 Veronica Huber <http://orcid.org/0000-0001-6304-3575>

#### REFERENCES

- Sung H, Ferlay J, Siegel RL, *et al.* Global Cancer Statistics 2020: GLOBOCAN Estimates of Incidence and Mortality Worldwide for 36 Cancers in 185 Countries. *CA Cancer J Clin* 2021;71:209–49.
- Li H, Boakye D, Chen X, *et al.* Association of Body Mass Index With Risk of Early-Onset Colorectal Cancer: Systematic Review and Meta-Analysis. *Am J Gastroenterol* 2021;116:2173–83.
- Fernández LP, Gómez de Cedrón M, Ramírez de Molina A. Alterations of Lipid Metabolism in Cancer: Implications in Prognosis and Treatment. *Front Oncol* 2020;10:577420.
- Pagès F, Mlecnik B, Marliot F, *et al.* International validation of the consensus Immunoscore for the classification of colon cancer: a prognostic and accuracy study. *Lancet* 2018;391:2128–39.

- Sillo TO, Beggs AD, Morton DG, *et al.* Mechanisms of immunogenicity in colorectal cancer. *Br J Surg* 2019;106:1283–97.
- Yang Y, Li L, Xu C, *et al.* Cross-talk between the gut microbiota and monocyte-like macrophages mediates an inflammatory response to promote colitis-associated tumorigenesis. *Gut* 2020;70:1495–506.
- James KR, Gomes T, Elmentaite R, *et al.* Distinct microbial and immune niches of the human colon. *Nat Immunol* 2020;21:343–53.
- Viola MF, Boeckxstaens G. Niche-specific functional heterogeneity of intestinal resident macrophages. *Gut* 2021;70:1383–95.
- Blériot C, Chakarov S, Ginhoux F. Determinants of Resident Tissue Macrophage Identity and Function. *Immunity* 2020;52:957–70.
- Bernardo D, Marin AC, Fernández-Tomé S, *et al.* Human intestinal pro-inflammatory CD11chighCCR2+CX3CR1+ macrophages, but not their tolerogenic CD11c–CCR2–CX3CR1– counterparts, are expanded in inflammatory bowel disease. *Mucosal Immunol* 2018;11:1114–26.
- Caprara G, Allavena P, Erreni M. Intestinal Macrophages at the Crossroad between Diet, Inflammation, and Cancer. *Int J Mol Sci* 2020;21:4825.
- Castoldi A, Monteiro LB, van Teijlingen Bakker N, *et al.* Triacylglycerol synthesis enhances macrophage inflammatory function. *Nat Commun* 2020;11:4107.
- Su P, Wang Q, Bi E, *et al.* Enhanced Lipid Accumulation and Metabolism Are Required for the Differentiation and Activation of Tumor-Associated Macrophages. *Cancer Res* 2020;80:1438–50.
- Chistiakov DA, Melnichenko AA, Myasoedova VA, *et al.* Mechanisms of foam cell formation in atherosclerosis. *J Mol Med* 2017;95:1153–65.
- Guerrini V, Prideaux B, Blanc L, *et al.* Storage lipid studies in tuberculosis reveal that foam cell biogenesis is disease-specific. *PLoS Pathog* 2018;14:e1007223.
- Guerrini V, Gennaro ML. Foam Cells: One Size Doesn't Fit All. *Trends Immunol* 2019;40:1163–79.
- Józefczuk J, Woźniewicz BM. Diagnosis and therapy of microscopic colitis with presence of foamy macrophages in children. *ISRN Gastroenterol* 2011;2011:756292.
- Wu H, Han Y, Rodriguez Sillke Y, *et al.* Lipid droplet-dependent fatty acid metabolism controls the immune suppressive phenotype of tumor-associated macrophages. *EMBO Mol Med* 2019;11:e10698.
- Rabold K, Aschenbrenner A, Thiele C, *et al.* Enhanced lipid biosynthesis in human tumor-induced macrophages contributes to their protumoral characteristics. *J Immunother Cancer* 2020;8:e000638.
- Veglia F, Tyurin VA, Mohammadyani D, *et al.* Lipid bodies containing oxidatively truncated lipids block antigen cross-presentation by dendritic cells in cancer. *Nat Commun* 2017;8:2122.
- Domanska D, Majid U, Karlsen VT, *et al.* Single-cell transcriptomic analysis of human colonic macrophages reveals niche-specific subsets. *J Exp Med* 2022;219:e20211846.
- Mantovani A, Allavena P, Marchesi F, *et al.* Macrophages as tools and targets in cancer therapy. *Nat Rev Drug Discov* 2022;21:799–820.
- Casiraghi E, Cossa M, Huber V, *et al.* MIAQuant, a novel system for automatic segmentation, measurement, and localization comparison of different biomarkers from serialized histological slices. *Eur J Histochem* 2017;61:2838.
- Casiraghi E, Huber V, Frasca M, *et al.* A novel computational method for automatic segmentation, quantification and comparative analysis of immunohistochemically labeled tissue sections. *BMC Bioinformatics* 2018;19:357.
- Bain CC, Scott CL, Uronen-Hansson H, *et al.* Resident and pro-inflammatory macrophages in the colon represent alternative context-dependent fates of the same Ly6Chi monocyte precursors. *Mucosal Immunol* 2013;6:498–510.
- Elmentaite R, Kumasaka N, Roberts K, *et al.* Cells of the human intestinal tract mapped across space and time. *Nature New Biol* 2021;597:250–5.
- Shaw TN, Houston SA, Wemyss K, *et al.* Tissue-resident macrophages in the intestine are long lived and defined by Tim-4 and CD4 expression. *J Exp Med* 2018;215:1507–18.
- Baghdadi M, Yoneda A, Yamashina T, *et al.* TIM-4 glycoprotein-mediated degradation of dying tumor cells by autophagy leads to reduced antigen presentation and increased immune tolerance. *Immunity* 2013;39:1070–81.
- Tse K, Ley K. Transforming growth factor- $\beta$ : transforming plaque to stability. *Eur Heart J* 2013;34:3684–6.
- Battle E, Massagué J. Transforming Growth Factor- $\beta$  Signaling in Immunity and Cancer. *Immunity* 2019;50:924–40.
- Luca BA, Steen CB, Matusiak M, *et al.* Atlas of clinically distinct cell states and ecosystems across human solid tumors. *Cell* 2021;184:5482–96.



- 32 Vernieri C, Fucà G, Ligorio F, *et al.* Fasting-Mimicking Diet Is Safe and Reshapes Metabolism and Antitumor Immunity in Patients with Cancer. *Cancer Discov* 2022;12:90–107.
- 33 Mariathasan S, Turley SJ, Nickles D, *et al.* TGF $\beta$  attenuates tumour response to PD-L1 blockade by contributing to exclusion of T cells. *Nature New Biol* 2018;554:544–8.
- 34 Lind H, Gameiro SR, Jochems C, *et al.* Dual targeting of TGF- $\beta$  and PD-L1 via a bifunctional anti-PD-L1/TGF- $\beta$ RII agent: status of preclinical and clinical advances. *J Immunother Cancer* 2020;8:e000433.
- 35 Bruni D, Angell HK, Galon J. The immune contexture and Immunoscore in cancer prognosis and therapeutic efficacy. *Nat Rev Cancer* 2020;20:662–80.
- 36 Bortolomeazzi M, Keddar MR, Montorsi L, *et al.* Immunogenomics of Colorectal Cancer Response to Checkpoint Blockade: Analysis of the KEYNOTE 177 Trial and Validation Cohorts. *Gastroenterology* 2021;161:1179–93.
- 37 Mennonna D, Maccalli C, Romano MC, *et al.* T cell neopeptide discovery in colorectal cancer by high throughput profiling of somatic mutations in expressed genes. *Gut* 2017;66:454–63.
- 38 Yang C, Wei C, Wang S, *et al.* Elevated CD163<sup>+</sup>/CD68<sup>+</sup> Ratio at Tumor Invasive Front is Closely Associated with Aggressive Phenotype and Poor Prognosis in Colorectal Cancer. *Int J Biol Sci* 2019;15:984–98.
- 39 Bain CC, Bravo-Blas A, Scott CL, *et al.* Constant replenishment from circulating monocytes maintains the macrophage pool in the intestine of adult mice. *Nat Immunol* 2014;15:929–37.
- 40 Almeida L, Everts B. Fa(c)t checking: How fatty acids shape metabolism and function of macrophages and dendritic cells. *Eur J Immunol* 2021;51:1628–40.
- 41 Di Conza G, Tsai C-H, Gallart-Ayala H, *et al.* Tumor-induced reshuffling of lipid composition on the endoplasmic reticulum membrane sustains macrophage survival and pro-tumorigenic activity. *Nat Immunol* 2021;22:1403–15.
- 42 Jaitin DA, Adlung L, Thaiss CA, *et al.* Lipid-Associated Macrophages Control Metabolic Homeostasis in a Trem2-Dependent Manner. *Cell* 2019;178:686–98.
- 43 Pascual G, Avgustinova A, Mejetta S, *et al.* Targeting metastasis-initiating cells through the fatty acid receptor CD36. *Nature New Biol* 2017;541:41–5.
- 44 Ou H-X, Guo B-B, Liu Q, *et al.* Regulatory T cells as a new therapeutic target for atherosclerosis. *Acta Pharmacol Sin* 2018;39:1249–58.
- 45 Peranzoni E, Lemoine J, Vimeux L, *et al.* Macrophages impede CD8 T cells from reaching tumor cells and limit the efficacy of anti-PD-1 treatment. *Proc Natl Acad Sci U S A* 2018;115:E4041–50.
- 46 Sugiyama D, Nishikawa H, Maeda Y, *et al.* Anti-CCR4 mAb selectively depletes effector-type FoxP3+CD4<sup>+</sup> regulatory T cells, evoking antitumor immune responses in humans. *Proc Natl Acad Sci U S A* 2013;110:17945–50.
- 47 Machicote A, Belén S, Baz P, *et al.* Human CD8+HLA-DR+ Regulatory T Cells, Similarly to Classical CD4+Foxp3+ Cells, Suppress Immune Responses via PD-1/PD-L1 Axis. *Front Immunol* 2018;9:2788.
- 48 Cohen SB, Maurer KJ, Egan CE, *et al.* CXCR3-dependent CD4<sup>+</sup> T cells are required to activate inflammatory monocytes for defense against intestinal infection. *PLoS Pathog* 2013;9:e1003706.
- 49 Medina-Contreras O, Geem D, Laur O, *et al.* CX3CR1 regulates intestinal macrophage homeostasis, bacterial translocation, and colitogenic Th17 responses in mice. *J Clin Invest* 2011;121:4787–95.
- 50 Rossini V, Zhurina D, Radulovic K, *et al.* CX3CR1<sup>+</sup> cells facilitate the activation of CD4 T cells in the colonic lamina propria during antigen-driven colitis. *Muc Immunol* 2014;7:533–48.